中国光学（中英文）
Chinese Optics
核心期刊

Development of visible/near-infrared multiband laser filter film

XIN Ya-wu, PENG Yong-chao, ZHANG Yu-xiang, CAO Xing-yu, HAN Yang, GUO Hong-ling, XIONG Shi-fu, HU Zhang-gui

文章编号　2097-1842(2026)01-0239-11

Development of visible/near-infrared multiband laser filter film

XIN Ya-wu[1], PENG Yong-chao[1], ZHANG Yu-xiang[1], CAO Xing-yu[1], HAN Yang[2], GUO Hong-ling[3], XIONG Shi-fu[1*], HU Zhang-gui[1]

(1. *State Key Laboratory of Crystal Materials*, *Tianjin Key Laboratory of Functional Crystal Materials*, *Institute of Functional Crystals*, *Tianjin University of Technology*, *Tianjin* 300384, *China*;
2. *Beijing Golden Way Scientific Co.*, *Ltd.*, *Beijing* 100015, *China*;
3. *Tianjin Key Laboratory of Film Electronic* & *Communication Devices*, *School of Integrated Circuit Science and Engineering*, *Tianjin University of Technology*, *Tianjin* 300384, *China*)

* *Corresponding author*, *E-mail*: *xsf_optics@126.com*

Abstract: Filters, as a key component in the photoelectric detection system, can simplify the optical system and improve detection efficiency. Based on the usage requirements, a visible/near-infrared filter film with up to 5 wavebands needs to be designed and prepared, while simultaneously satisfying high reflection in 2 wavebands and high transmittance in 3 wavebands. Therefore, we have conducted a systematic study on the film design, thin film preparation process, and control accuracy of film layer thickness. In this work, the short-wave pass film system is superimposed with the long-wave pass film system, and the number of cycles and matching coefficient of the film system are tuned to meet the requirements of cut-off band. Additionally, Smith method was used to match bandpass film system to optimize the transmission band and complete the visible/near infrared multiband laser filter film design. In the preparation process, combined with the sensitivity of the film layer, inverse analysis is used to invert the film layer monitored by each optical monitoring chip. The optical control scheme with weak optical signal in the monitoring process is simulated and corrected, and the monitoring wavelength with stronger optical signal is matched, resulting in an improvement of the control accuracy for the film thickness and the transmittance in the specified wavelength range. Ultimately, the actual physical thickness is 9.66 μm, and the error with the theoretical design thickness is less than 0.4%, and the transmittance of the specified 3 wavebands exceeds 99%. The average transmittance of the cut-off bands at the 455−500 nm and 910−1 000 nm is 0.45% and 0.16%, respectively.

Key words: optical film; multiband; film system design; reverse analysis

收稿日期:2025-05-11; **修订日期**:2025-06-04
基金项目:国家自然科学基金(No. 62304152)
Supported by the National Natural Science Foundation of China (No. 62304152)

可见/近红外多波段激光滤光膜的研制

辛亚武[1], 彭永超[1], 张宇翔[1], 曹兴宇[1], 韩　阳[2], 郭洪玲[3], 熊仕富[1*], 胡章贵[1]
（1. 天津理工大学 功能晶体研究院 晶体材料全国重点实验室 天津市功能晶体材料重点实验室, 天津 300384；
2. 北京欧普特科技有限公司, 北京 100015；
3. 天津理工大学 集成电路科学与工程学院 天津市薄膜电子与通信器件重点实验室, 天津 300384）

摘要: 滤光片作为光电探测系统中的关键部件, 能够简化光学系统并提高探测效率。根据使用需求, 需要设计并制备出一种多达 5 个波段的可见/近红外滤光膜, 同时满足 2 个波段高反射和 3 个波段高透过的要求。因此, 本文对膜系设计、薄膜制备工艺以及膜层厚度的控制精度进行了系统研究。在本工作中, 将短波通膜系与长波通膜系进行叠加, 并调整膜系的周期数和匹配系数, 以满足截止波段的要求。此外, 运用 Smith 方法优化带通膜系透过波段, 从而完成可见/近红外多波段激光滤光膜的设计。在制备过程中, 结合膜层的灵敏度, 通过反演分析各光学监控片所监控的膜层。对监控过程中光信号较弱的光学监控方案进行模拟和修正, 并匹配光信号较强的监控波长, 进而提高了膜层厚度的控制精度以及在指定波长范围内的透过率。最终, 制备的滤光膜实际物理厚度为 9.66 μm, 与理论设计厚度的误差小于 0.4%, 且 3 个透过波段的透过率均超过 99%。在 455~500 nm 和 910~1 000 nm 波段的平均透过率分别为 0.45% 和 0.16%。

关　键　词: 光学薄膜; 多波段; 薄膜系统设计; 逆向分析

中图分类号: O482.31　　**文献标志码:** A　　**doi:** 10.37188/CO.EN-2025-0031　　**CSTR:** 32171.14.CO.EN-2025-0031

1 Introduction

In recent years, with the rapid development of laser systems[1-2], optical microcavity[3-4], optical communication and biological detection[5-9], the used instruments have put forward higher requirements for the optical performance of the optical system filter. The design process is complicated and the optical path is intricate by selecting a variety of single-band spectral filters to overlap according to different bands, rendering the single-band spectral filter inadequate for meeting the needs of using requirements. In contrast, multiband filter films offer advantages such as simplifying the optical path mechanism design and enhancing the detection efficiency, making them widely used in optical microcavities, biological detection and other fields.

In 2014, Tongtong Wang et al. designed and prepared dual-band infrared antireflection film, which could achieve an average transmittance of more than 95% in the 0.8−1.7 μm and 3.7−4.8 μm bands[10]. In 2016, Gaoyuan Mi et al. designed a triple-band antireflection film, which was able to achieve an average transmittance of more than 96.0% in the 0.5−0.8 μm, 1.064 μm, and 3.7−4.8 μm bands[11]. John C. Bellum et al. developed a 22.5° dichroic color-splitting film with 96.6% and 0.6% transmittance at 527 nm and 1 054 nm, respectively[12]. By 2022, a study produced three-band compatible high reflectance dielectric films with an average reflectance of more than 99.5% in the bands of 0.5−0.65 μm, 0.78−0.83 μm, and 1.05−1.08 μm[13]. Xingyu Chen et al. developed a five-band antireflection film, which finally achieved transmittance over 91.0% at 0.808 μm, 0.880 μm, 0.915 μm, and more than 95% at 3.7−4.8 μm and 10.6 μm[14]. Using TiO_2 and SiO_2 as coating materials, spectroscopic films were prepared, yielding transmittance of 10.3%, 10.5% and 80.4% at 0.4 μm, 0.68 μm and 0.485 μm, respectively[15]. It can be concluded that researchers have conducted extensive studies on the design and preparation of multiband filter films, but there are few reports on filter films with up to five bands.

The developed multiband laser filter in this work covers the visible and near-infrared spectral regions. Due to the simultaneous reflection and transmission of multiband, there are high requirements for the design of the film system, the film preparation process, and the control accuracy of the film thickness. In this work, based on the requirements of technical parameters, a reasonable film system scheme is designed with suitable high and low refractive index coating materials, and the monitoring scheme of high sensitivity film layer is optimized, and physical vapor deposition (PVD) technology is used to prepare multiband laser filter film.

2 Experiment

2.1 Materials and software

In this work, BK7 is selected as the substrate material for the filter due to its excellent light transmittance, stable physical and chemical properties, and good mechanical strength. The specific dimensions are 1 inch in diameter and 4 mm in thickness. The specific technical parameters of the film are shown in Table 1.

Tab. 1 Technical parameters of multiband laser filter film

Parameter	Specification
Angle /°	0
Transmission band /nm	880, 1 064, 1 083, 1 342
Transmittance /%	⩾99
Waveband of cut−off region /nm	455-500; 910-1 000
Transmittance of cut−off region /%	<1

Based on the analysis of technical parameters, the coating material with a transparent region of 400−1 400 nm band could be selected. Within this spectral range, commonly employed materials include TiO_2, H4, Ta_2O_5 and HfO_2. In the vacuum heating and evaporation, TiO_2 is prone to loss of oxygen due to the decomposition, generating high absorption sub-titanium oxide thin film Ti_nO_{2n-1} ($n = 1, 2, \cdots, 10$) and affecting the stability of the coating. Under the electron beam heating and evaporation, the refractive index of H4 and HfO_2 are lower than Ta_2O_5, and Ta_2O_5 film has a dense film structure, low absorption characteristics and strong laser damage resistance[16-17]. Consequently, Ta_2O_5 has been used as the high refractive index film layer material. SiO_2 film has the characteristics of low compressive stress, high damage threshold, and robust layer integrity. As an oxide compatible as Ta_2O_5, SiO_2 was selected as the material of low refractive index film layer in this work.

The coating materials used in the experiment include Ta_2O_5 (99.998%, JuBo Guneng (Suzhou) Thin Film Materials Co., Ltd.) and SiO_2 (99.999 7%, JuBo Guneng (Suzhou) Thin Film Materials Co., Ltd.). OptiLayer (13.77, OptiLayer GmbH, Russia) software was used to design the film system and analyze the sensitivity of each film layer. MCalc (V4.0.21, Leybold Optics (Beijing) Co., Ltd.) software was used to calculate optical constants of the films and design the optical control monitoring scheme.

2.2 Thin film preparation

Thin film preparation was conducted on a Leybold SYRUSpro1110 vacuum coating machine, employing a dual e-type electron gun to facilitate the evaporation of the material, an APS ion source to assist deposition, and an OMS5100 optical film thickness monitoring system and a six-probe crystal control system to monitor the thickness of the film and the rate of deposition of the material in real time throughout the experiment.

The actual plating process parameters resulting from the combination of material properties and equipment process parameters are presented in Table 2. Here, APS denotes the ion source, and HPE denotes the electron gun. Prior to depositing the film, the substrate is wiped with an ethanol ether mixture with a volume ratio of 1∶3. After the program is set up, the substrate was baked at 180 °C for 1 800 s when the vacuum degree reaches 5×10^{-5} mbar. After baking, the APS ion source is turned on and the surface of the substrate is bombarded for 300 s, and then the coating is started.

After deposition of the film, the vacuum chamber is cooled down to room temperature and the samples are removed.

Tab. 2 Equipment process parameters

Material	Substrate temperature/°C	Degree of vacuum/mbar	Deposition rate/nm·s^{-1}	Flow rate of O_2/sccm	
				APS	HPE
Ta_2O_5	180	5×10^{-5}	0.3	15	35
SiO_2			0.7	25	25

2.3 Characterization

The transmittance of the films coated was tested using an UV-Vis spectrophotometer (Cary-7000, Agilent, USA). The surface shape of the substrates with deposited film was characterized by a laser interferometer (G150, Shine Optics, China) with the light source wavelength of 632.8 nm. The cross-sectional morphology of the films was measured by an environmental field-emission scanning electron microscope (Quanta FEG 250, FEI, USA).

3 Results and discussion

3.1 Film system design

The analysis of technical parameters indicates that the film system needs to satisfy the two reflection bands and four transmission bands. According to the theory of thin film design, the first step in the design process is to establish the reflection band, which then be calculated by the characteristic matrix method[18]. The characteristic matrix of the periodic film is shown in formula (1) and (2)

$$\boldsymbol{M}_1=\begin{bmatrix}\cos\delta_1 & \dfrac{i}{\eta_1}\sin\delta_1\\ i\eta_1\sin\delta_1 & \cos\delta_1\end{bmatrix}\quad,\tag{1}$$

$$\boldsymbol{M}_2=\begin{bmatrix}\cos\delta_2 & \dfrac{i}{\eta_2}\sin\delta_2\\ i\eta_2\sin\delta_2 & \cos\delta_2\end{bmatrix}\quad,\tag{2}$$

where δ_1, δ_2 denote the phase difference of high and low refractive index materials, respectively. η_1, η_2 denote the refractive indices of high and low refractive index materials, respectively. Assuming that the film system repeated periods is s, the characteristic matrix of the film system can be obtained as

$$\mu=\boldsymbol{M}^s\quad,\tag{3}$$

where $\boldsymbol{M}$ is a fundamental cycle of periodic film system and the characteristic matrix can be written as

$$\boldsymbol{M}=\boldsymbol{M}_1\boldsymbol{M}_2\boldsymbol{M}_1\boldsymbol{M}_2\cdots\boldsymbol{M}_1\boldsymbol{M}_2\boldsymbol{M}_1=\begin{bmatrix}m_{11} & m_{12}\\ m_{21} & m_{22}\end{bmatrix}.\tag{4}$$

Matrix operations are performed and it can be obtained that

$$m_{11}=m_{22}=\cos2\delta_1\cos\delta_2-\frac{1}{2}\left(\frac{\eta_1}{\eta_2}+\frac{\eta_2}{\eta_1}\right)\sin2\delta_1\sin\delta_2,\tag{5}$$

$$m_{12}=\frac{i}{\eta_1}\begin{bmatrix}\sin2\delta_1\cos\delta_2+\dfrac{1}{2}\left(\dfrac{\eta_1}{\eta_2}+\dfrac{\eta_2}{\eta_1}\right)\cos2\delta_1\sin\delta_2+\\ \dfrac{1}{2}\left(\dfrac{\eta_1}{\eta_2}-\dfrac{\eta_2}{\eta_1}\right)\sin\delta_1\end{bmatrix},\tag{6}$$

$$m_{21}=i\eta_1\begin{bmatrix}\sin2\delta_1\cos\delta_2+\dfrac{1}{2}\left(\dfrac{\eta_1}{\eta_2}+\dfrac{\eta_2}{\eta_1}\right)\cos2\delta_1\sin\delta_2+\\ \dfrac{1}{2}\left(\dfrac{\eta_1}{\eta_2}-\dfrac{\eta_2}{\eta_1}\right)\sin\delta_1\end{bmatrix}.\tag{7}$$

If $|1/2(m_{11}+m_{22})|>1$, the equivalent conductance is imaginary, that is, the waveband is a reflection band when there are enough film layers and the width of the reflection band wave number Δg is

$$\Delta g=\frac{2}{\pi}\arcsin\left(\frac{\eta_1-\eta_2}{\eta_1+\eta_2}\right)\quad.\tag{8}$$

Therefore, the reflective band boundary wavelength λ_1 and λ_2 can be calculated as

$$\lambda_1=\frac{\lambda_0}{1+\Delta g},\lambda_2=\frac{\lambda_0}{1-\Delta g}\quad.\tag{9}$$

Thus, the wavelength width of the reflective band $\Delta\lambda$ is

$$\Delta\lambda=2\Delta g\lambda_0\quad.\tag{10}$$

The reflection bandwidths with center wavelengths of 475 nm and 950 nm are calculated by equations (9) and (10). The long-wavelength-passing film system Sub|(0.5HL0.5H)^S_1|Air is employed as the fundamental structure, with S_1 representing the number of cycles, Sub representing the substrate, Air representing the incident medium, H and L representing the λ/4 optical thickness of Ta_2O_5 and SiO_2, respectively, and λ representing the reference wavelength. The superimposition of a short wave pass film system Sub|(LHL)^S_2|Air onto the film system structure is overlapped with the long wave pass film system. Simultaneously, the number of film system periods and matching coefficients are tuned to set up the two reflection bands for shortwave and longwave.

According to the reflective bandwidth of the film system and the reference wavelength, combined with OptiLayer software to simulate the theoretical value of the spectrum of the film system, the period numbers of the two film stacks is tuned to investigate the dependency of the reflectivity on the period numbers, and the result is shown in Fig. 1(a) and (b) (color online). The transmittance in the bands of 455−500 nm and 910−1 000 nm is high when the period number is small and decreases with the increase of the period numbers. The specific theoretical values in relation to the period number are shown in Table 3. Considering the increasing number of film layers with the period numbers, the passband waviness will increase, and the subsequent compression of the waviness and the fabrication complexity will also rise. After comprehensive evaluation, S_1=8 and S_2=15 were selected as two film stack cycle, as demonstrated in Fig. 1(c) (color online). The 455−500 nm and 910−1 000 nm exhibit high degree of cut-off, and the transmission region maintains excellent transparency.

Under the premise of ensuring the spectral characteristics of the cut-off band, it is necessary to design the transmission band to meet the subsequent optimized transmission spectral curve with high passband transmission, high rectangularity. The film system structure of the transmission band is designed according to Smith's method, and the film system structure expression is Sub|[n(HL)^sH 2ωL n(HL)^sH ωL)]^S_3|Air. The method involves treating the film stack on either side of the selecting layer as two effective interfaces, typically, with spacer layer composed of 2ωL or 2ωH.

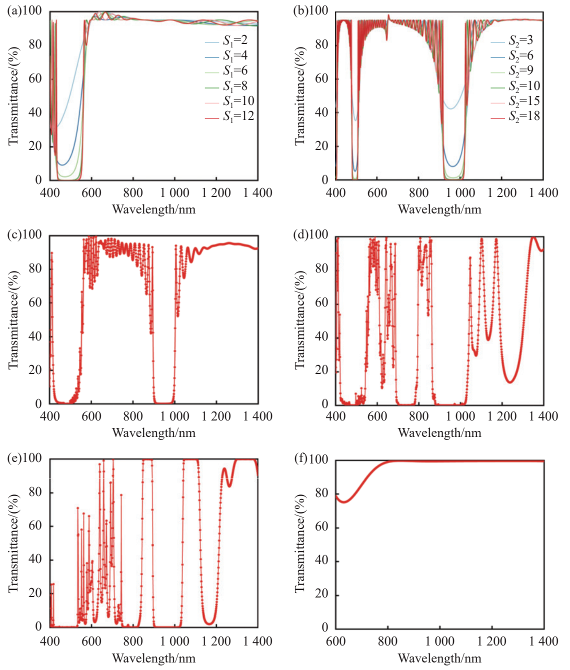

Fig. 1 Transmittance spectral curves of (a) long-wavelength-passing and (b) short-wavelength-passing with different period numbers; (c) superimposed transmittance spectral curves of film system at period number S_1=8, S_2=15; (d) initial design and (e) optimized design transmittance spectral curve; (f) transmittance spectral curve of antireflection film

Tab. 3 Spectral theoretical values and period numbers

Cycles number of S_1	$T_{455\text{-}500\ nm}$ /%	Cycles number of S_2	$T_{910\text{-}1000\ nm}$ /%
2	43.23	3	44.66
4	10.68	6	12.49
6	2.42	9	5.70
8	0.56	12	0.87
10	0.13	15	0.12
12	0.02	18	0.07

At the center wavelength and adjacent wavelength, transmission peaks appear. Then, the equivalent refractive index is adjusted after a reasonable symmetrical matching of high and low refractive index materials to generate transmission band in the desired wavelength band. According to the interference results of the effective interface, the distribution of the total interface transmittance can be derived by formula (11)

$$T = \frac{T_1T_2}{[1-(R_1R_2)^{1/2}]^2\left[1+\frac{4(R_1R_2)^{1/2}}{(1-R_1R_2)^{1/2}}\sin^2\left(\frac{\varphi_1+\varphi_2-2\delta}{2}\right)\right]}, \tag{11}$$

where T_1, T_2, R_1, R_2 are the transmittance and reflectance of the two reflective stacks, respectively, φ_1 and φ_2 are the phase of the two film stacks, respectively, and δ is the effective phase thickness. Near the transmission peak wavelength in the film system, a better passband shape can be obtained by using a film system with a rapid change in reflectivity. According to equation (11), it can be seen that when R_1=R_2, the phase condition is

$$\frac{\varphi_1+\varphi_2-2\delta}{2} = m\pi \quad , \tag{12}$$

then high transmittance is obtained at any wavelength.

The single cavity is connected in series in the basic spectrum of the multi-band filter film. Among them, the parameters such as the matching number s of high and low refractive index materials, the coefficient n, and the interval layer coefficient 2ω in each single cavity reflection layer determine the bandwidth of passband. The spectra of film systems with varying coefficients are simulated, and it is observed that the coefficient ω affects the passband spacing, which increases with ω. However, the amplitude of the passband ripples at the center wavelength increases as ω increases. The coefficient n affects the passband bandwidth. As n increases, the passband becomes wider, but the cut-off degree in the inter-passband cut-off region becomes worse. Increasing the number of single cavities [*n*(*HL*)^*s* *H*] in the film system can increase the number of passbands, while the bandwidth of each passband becomes narrower.

The target band was adjusted, and multiple simulations were conducted to determine the optimal parameters for s=1, n=1, ω=1 and S_3=5. The film system Sub|(*HLH* 2*L* *HLH* *L*)^5 |Air can be obtained, which ensures that the cut-off region is not destroyed and the transmission peaks appear in the passband. The subsequent optimization process can be also simplified. Initial transmittance curve for the film system is obtained as shown in Fig. 1(d) (color online).

As illustrated in Fig. 1(d), the amplitude of the ripple oscillation in the passband is large. To fulfill the technical specifications, it is imperative to implement effective measures for passband ripple compression and to optimize the overall design of the film system. The film system is input into the OptiLayer software to optimize the design of the film system. In the process of establishing the target parameters for optimization, the introduction of an unregulated film layer serves to compress the passband interval ripples and enhance the passband transmittance. The final film system was obtained as Sub|0.3921*H* 0.1512*L* 0.3712*H* 0.3958*L*···1.6621*L* 0.9022*H* 0.2846*L* 0.4560*H* |Air, with a total of 85 layers and a physical thickness of 9.69 μm, and the transmittance spectral curves of the optimized film system are shown in Fig. 1(e) (color online). The optimized film system exhibits a high cut-off rate in the cut-off region and a smooth ripple compression in the passband range. The transmittance at 880 nm, 1 064 nm, 1 083 nm, and 1 342 nm is 99.90%, 99.99%, 99.99%, and 99.97%, respectively. The transmittance at 455−500 nm and 910−1 000 nm is 0.01% and 0.003%, respectively. The design meets the technical specifications with significantly enhanced transmittance in the passband region and better suppression of passband ripple oscillations.

To ensure that the light output is maintained at a high transmittance rate, an antireflection film with a wavelength range of 800-1 400 nm needs to be deposited on the other side of the substrate. The design scheme of the antireflection film was Sub|0.4597*H* 0.6382*L* 3.8605*H* 1.7642*L*|Air, comprising a total of four layers of film with a physical thickness of approximately 548.54 nm. The transmittance curve of the designed antireflection film is illustrated in Fig. 1(f). Given the antireflective coating has a relatively simple design due to fewer layers, the development process of antireflection film is not described in detail in this work.

3.2 Film thickness monitoring scheme

This work follows film thickness control scheme previously reported by us, which involves a combination of "crystal control with optical control". The crystal control method involves monitoring the physical thickness of the film by monitoring the amount of change in the vibration frequency of the quartz crystals of the AT cut, enabling the real-time detection of the film deposition rate. The optical control method employs the changes in light intensity or polarization state of transmitted or reflected light caused by thin film interference inventively to determine the optical thickness of the film, incorporating a compensation mechanism for the film thickness error.

The designed film system parameters were imported into MCalc software for simulating and optimizing the parameters including the number of optical control chip and monitoring wavelength. It was determined that controlling the error of each layer within 1% is unfeasible when the number of optical control chips is less than 3. Therefore, it was concluded that the optimal number of optical control chips in this scheme is 3, as illustrated in Fig. 2 (color online). The first optical control chip monitors 1st-32nd layers, with a monitoring wavelength of 660 nm. The second optical control chip monitors 33rd-68th layers, with a monitoring wavelength of 664 nm. The third optical control chip monitors 69th-85th layers, with a monitoring wavelength of 688 nm.

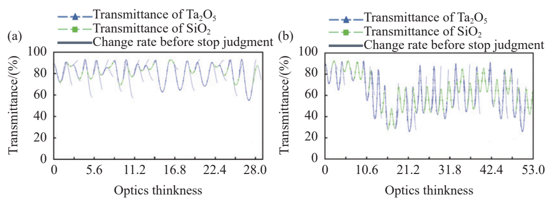

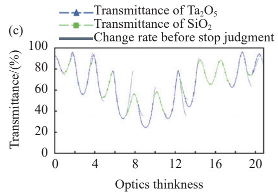

Fig. 2 Optical monitoring design of multiband laser filter film. (a) 1#; (b) 2#; (c) 3#

3.3 Spectral testing and analysis

Transmittance measurements were performed on the deposition films and the results are shown in Fig. 3(a) (color online). It was found that the average transmittance in the cut-off region of the 455−500 nm and 910−1 000 nm bands was 1.04% and 0.36%, respectively. In contrast, the passband transmittance had decreased significantly, with transmittance at 880 nm, 1 064 nm, 1 083 nm, and 1 342 nm being 81.86%, 91.91%, 94.65%, and 95.69%, respectively.

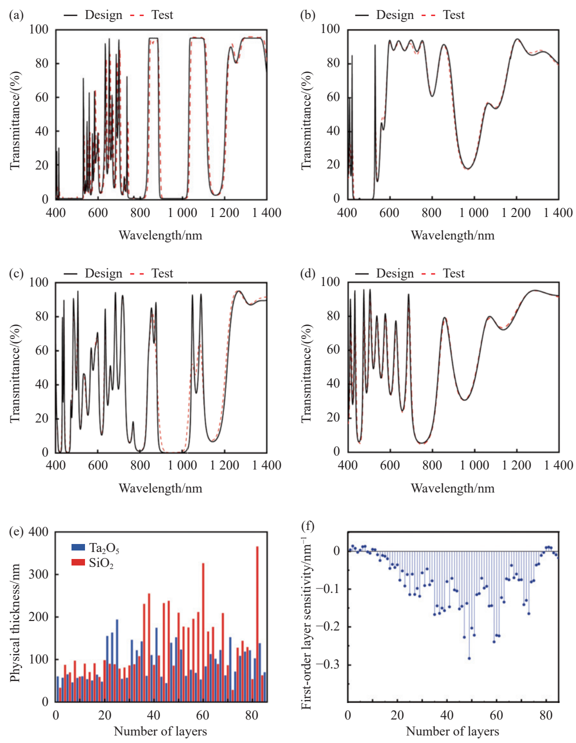

Fig. 3 (a) Measured and designed transmittance spectral curve of film; measured and designed transmittance spectral curves for optical control chips (b) 1#, (c) 2#, (d) 3#; (e) physical thickness of the film layer; (f) sensitivity of the film layer

By analyzing the discrepancy between the deposition thickness of each layer of the film system and the designed thickness in the experiment, it is found that several film layers showed significant deviation. Therefore, the spectral testing for optical control chips ($1^{\#}$, $2^{\#}$ and $3^{\#}$) and interactive analysis with the theoretical design were conducted on them accordingly. The results of the testing and analysis are presented in Fig. 3(b−d) (color online).

The actual coating process is subject to a number of variables, including temperature, vacuum, deposition rate, which result in slight variations to the theoretical design in the preparation of each layer of film. The test spectra of the $1^{\#}$ and $3^{\#}$ optical control chip exhibited minimal discrepancy with the theoretical design, whereas the transmittance curve of the film layer monitored by the $2^{\#}$ optical control chip demonstrated a notable decline. This is due to the weak optical signal during wavelength monitoring, which prevents the film system from meeting the expected standards.

By employing reverse engineering software to analyze the discrepancy between the actual and designed thickness of each layer of the film system, it was determined that among the 33rd-68th layers monitored by the $2^{\#}$ optical control chip, the actual plating thickness of the 38th, 49th, 50th, and 60th layers deviate from the designed thickness seriously.

The thickness of each layer of the film and its sensitivity were analyzed using OptiLayer software, as illustrated in Fig. 3(e) and (f) (color online). This software enables precise error assessment during preparation by quantifying how thickness control deviations, with larger sensitivity values resulting in greater impact on the transmittance spectrum of the film system. This can potentially cause negative effects such as " collapse" in the spectral transmittance region and "uneven" characteristics, leading to a discrepancy between the actual transmittance curve and the theoretical design. Consequently, it is imperative to exercise precise control over the highly sensitive film layer to obtain results that are in accordance with the theoretical design.

Therefore, in conjunction with the film layer sensitivity analysis, $2^{\#}$ optical monitoring scheme needs to be adjusted. The film system parameters are imported into the MCalc software for the simulation of the optical control scheme, adjusting the $2^{\#}$ optical monitoring wavelength, comparing and analyzing the strength of the $2^{\#}$ optical signal as well as the degree of matching with the monitoring wavelengths of the $1^{\#}$ and $3^{\#}$ optical control chip. The monitoring wavelengths were closely matched to minimize the systematic error caused by the grating adjustment in the optical control system. After re-simulation of $2^{\#}$ optical monitoring scheme of 33rd-68th layers of film, and find a monitoring wavelength at 601 nm with a stronger optical signal was found, and the original monitoring program was replaced. The optical monitoring signal changing with the thickness for $2^{\#}$ optical monitoring scheme is shown in Fig. 4(a) (color online), and the error of each film layer thickness can be controlled to less than 0.5%. Re-depositing the 33rd-68th layers of films for $2^{\#}$ optical monitoring scheme, spectral tests results are shown in Fig. 4(b) (color online). It can be observed that transmittance in the 1 000−1 100 nm band of the adjusted $2^{\#}$ optical control chip is greatly improved and the error between transmittance spectral curve and theoretical design is smaller.

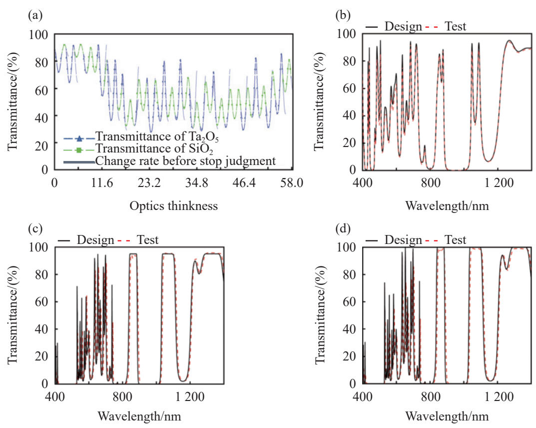

Fig. 4 Adjusted $2^{\#}$ optical monitoring. (a) Design scheme and (b) experimental test transmittance spectral curve; measured and design transmittance spectral curves for (c) single-sided and (d) double-sided films

Based on the optimization of the 2# optical control chip, the multiband laser filter film was completely coated again, and the spectral testing results are shown in Fig. 4(c). The average transmittance of the film samples in the cut-off region of 455−500 nm and 910−1 000 nm bands is 0.45% and 0.16%, respectively, and the transmittance in the transmission regions of 880 nm, 1 064 nm, 1 083 nm, and 1 342 nm is 94.91%, 95.05%, 95.06% and 95.08%, respectively. It can be concluded that the spectral characteristics of the transmission area have been significantly improved, leading to an increase in transmission rate. After depositing antireflective film on the other side of the sample, the spectral test of the double-sided coating is shown in Fig. 4(d). The average transmittance of the film samples in the cut-off region of 455−500 nm and 910−1 000 nm bands is 0.45% and 0.16%, respectively, and the transmittance in the transmission region of 880 nm, 1 064 nm, 1 083 nm and 1 342 nm is 99.13%, 99.04%, 99.04% and 99.07%, respectively, which can meet the requirements of the technical parameters.

3.4 SEM testing

The cross-sectional morphology of the multiband laser filter film was characterized using an environmental field-emission scanning electron microscope (SEM). By measuring the actually deposited film thickness via SEM cross-sectional imaging and comparing it with the designed value, the thickness error of the prepared film was determined, directly reflecting the deposition accuracy of the coating process. The SEM results in Fig. 5(a) (color online) show that the multiband laser filter film exhibits a distinct layered structure. The physical thickness of the film is 9.66 μm, with a relative error of 0.37% compared to the theoretical design value of 9.69 μm.

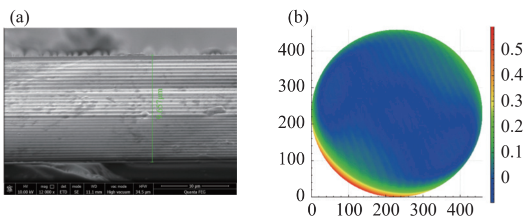

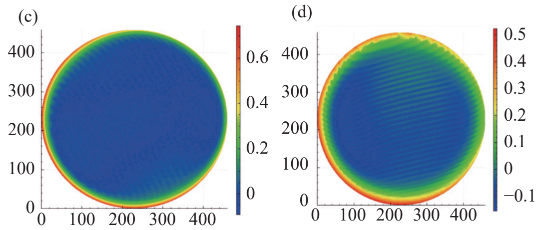

Fig. 5 (a) Cross-sectional morphology of multiband laser filter film. (b) Uncoated substrate surface shapes. (c) Single-sided coated surface shapes. (d) Double-sided coated surface shapes

3.5 Surface shape testing

Due to the difference between the film and the substrate material, along with the energetic particle bombardment during preparation, the microstructure of the film material deviates from the equilibrium state. This generates residual stress throughout the film structure, consequently causing microscopic morphology of the film surface irregularities. Here, a ZYGO laser interferometer was used to measure the surface shape of the substrate. The two parameters of the surface profile are PV (the difference between the wave peaks and troughs at the microlevel) and RMS (Root Mean Square of surface roughness), which reflect the flatness of the film surface. These parameters reflect the flatness of the film surface, and the light source wavelength of the interferometer is 632.8 nm. Fig. 5(b) (color online) shows the surface shape of the uncoated substrate with PV value of 0.234 58λ and RMS value of 0.021 48λ.

Fig. 5 (c) and (d) (color online) shows the surface shape test plots for single-sided and double-sided coatings. The measured PV values were 0.396 72λ and 0.678 18λ and the RMS values were 0.051 55λ and 0.115 65λ for single and double-sided coatings, respectively. As shown in the figure, the PV value gradually increases from the center to the edge of the coating, but all indicators meet the technical requirements within the effective clear aperture. Since the overall stress of double-sided coating is higher than that of single-side coating, the micro-morphology of double-sided coating is more inhomogeneous than that of single-sided coating. Although the deformation degree and surface roughness are higher than that of single-sided coating, overall, both the PV value and the RMS value satisfy the requirements for use.

4 Conclusion

In summary, according to the requirements of multi-band laser filter film, a visible/near-infrared multiband laser filter film is successfully developed by combining different film systems. The structure of multi-channel filter film system is analyzed and summarized, and the design method and the law of multi-channel filter film were identified. The sensitivity of each film layer of the filter film is inversed and analyzed using the reverse engineering software OptiRE, and the film thickness monitoring method is optimized. This, addressed the issue of excessive film layer error caused by optical monitoring during the deposition process. The average transmittance of the prepared filter film samples in the cut-off region of 455−500 nm and 910−1 000 nm bands is 0.45% and 0.16%, respectively. Moreover, the transmittance is 99.13%, 99.04%, 99.04%, and 99.07% at 880 nm, 1 064 nm, 1 083 nm, and 1 342 nm, respectively, which fulfill the requirements of the technical specifications.

References:

[1] ZHANG D H, DONG Z M, ZHANG CH, *et al*.. Investigation on parallel auxiliary adjusting machine of spatial filter lens for a high-power laser facility[J]. *Optics & Laser Technology*, 2022, 147: 107597.

[2] ZHANG J L, GAO G J, WANG B L, *et al*.. Background noise resistant underwater wireless optical communication using faraday atomic line laser and filter[J]. *Journal of Lightwave Technology*, 2022, 40(1): 63-73.

[3] CHEN X CH, LIANG P X, WU Q, *et al*.. Fluorescence enhanced optical resonator constituted of quantum dots and thin film resonant cavity for high-efficiency reflective color filter[J]. *Nanomaterials*, 2021, 11(11): 2813.

[4] ZHU H, XIN Y W, CHEN Y R, *et al*.. Development of resonant cavity film for 575 nm all-solid-state laser system[J]. *Coatings*, 2023, 13(7): 1278.

[5] SHAKTHI MURUGAN K H, SUMATHI M. Design and analysis of 5G optical communication system for various filtering operations using wireless optical transmission[J]. *Results in Physics*, 2019, 12: 460-468.

[6] GE P F, LING X T, WANG J H, *et al*.. Optical filter bank modeling and design for multi-color visible light communications[J]. *IEEE Photonics Journal*, 2021, 13(1): 7901219.

[7] NIKOLAIDOU K, CONDELIPES P G M, CANEIRA C F R, *et al*.. Monolithically integrated optical interference and absorption filters on thin film amorphous silicon photosensors for biological detection[J]. *Sensors and Actuators B: Chemical*, 2022, 356: 131330.

[8] LIU ZH X, TAO L T, ZHANG Y ZH, *et al*.. Narrowband near-infrared photodetector enabled by dual functional internal-filter-induced selective charge collection[J]. *Advanced Optical Materials*, 2021, 9(15): 2100288.

[9] BAN CH, GAO P, REN SH P, *et al*.. Design and manufacturing of filter sets for dual-color synchronous gene sequencing[J]. *Coatings*, 2023, 13(9): 1555.

[10] 王彤彤. 基于氧化物的 0.8~1.7μm 和 3.7~4.8μm 硬质宽带红外增透膜研制[J]. 中国光学, 2014, 7(5): 816-822.
WANG T T. Fabrication of hard infrared anti-reflection coating with broadband in the wavelength of 0.8~1.7 μm and 3.7~4.8 μm based on oxide material[J]. *Chinese Optics*, 2014, 7(5): 816-822. (in Chinese).

[11] 米高园, 张建付, 韩俊, 等. 电视、激光、中波红外多波段增透膜研究[J]. 激光与红外, 2016, 46(5): 593-596.
MI G Y, ZHANG J F, HAN J, *et al*.. Research on antireflection coating for TV, laser, mid-infrared wavebands[J]. *Laser & Infrared*, 2016, 46(5): 593-596. (in Chinese).

[12] BELLUM J C, FIELD E S, KLETECKA D E, *et al*.. Design and laser damage properties of a dichroic beam combiner coating for 22.5-deg incidence and S polarization with high transmission at 527 nm and high reflection at 1054 nm[J]. *Optical Engineering*, 2016, 56(1): 011020.

[13] 师云云, 徐均琪, 刘政, 等. 多波段大口径全介质高反膜的设计与制备[J]. 表面技术, 2022, 51(4): 335-341.
SHI Y Y, XU J Q, LIU ZH, *et al*.. Design and preparation of large aperture high reflective films composed entirely of

dielectric materials for multi-band application[J]. *Surface Technology*, 2022, 51(4): 335-341. (in Chinese).

[14] 陈星聿, 关冉昀, 张守立, 等. 硒化锌基底多波段红外增透膜的研究[J]. 光电技术应用, 2022, 37(6): 18-21,106.
CHEN X Y, GUAN R Y, ZHANG SH L, *et al*.. Study of multi-band infrared antireflection coatings on zinc selenide substrate[J]. *Electro-Optic Technology Application*, 2022, 37(6): 18-21,106. (in Chinese).

[15] KIM D, KIM K M, HAN H, *et al*.. Ti/TiO_2/SiO_2 multilayer thin films with enhanced spectral selectivity for optical narrow bandpass filters[J]. *Scientific Reports*, 2022, 12(1): 32.

[16] 范欢欢, 章岳光, 沈伟东, 等. 原子层沉积制备 Ta_2O_5 薄膜的光学特性研究[J]. 光学学报, 2011, 31(10): 1031001.
FAN H H, ZHANG Y G, SHEN W D, *et al*.. Optical properties of Ta_2O_5 thin films fabricated by atomic layer deposition[J]. *Acta Optica Sinica*, 2011, 31(10): 1031001. (in Chinese).

[17] SHANG P, XIONG SH M, LI L H, *et al*.. Investigation on thermal stability of Ta_2O_5, TiO_2 and Al_2O_3 coatings for application at high temperature[J]. *Applied Surface Science*, 2013, 285: 713-720.

Author Biographies：

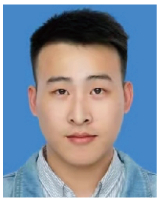

XIN Ya-wu (1999—), male, born in Zhoukou, Henan Province. He is currently a Master student at Tianjin University of Technology. He received his Bachelor of Engineering (B.E.) degree in Optoelectronic Information Science and Engineering from Nanyang Institute of Technology in 2022. His research interests focus on the design and fabrication of visible and infrared optical coatings. E-mail: xyw_optics@163.com

XIONG Shi-fu (1988—), male, born in Shiyan, Hubei Province. He is an assistant researcher at the Functional Crystal Institute of Tianjin University of Technology, where he is also the director of the crystal coating laboratory. He graduated from Changchun University of Science and Technology in 2018 with a Ph.D. in optical engineering, and his main research direction is the development and performance evaluation of precision optical thin films. E-mail: xsf_optics@126.com